Aust. J. Phys., 1992, **45**, 797–817

Observations of Southern Radio Galaxies at 1415 MHz

P. A. Jones

School of Physics, University of Sydney,
Sydney, N.S.W. 2006, Australia.

Abstract

The structures of 23 strong radio galaxies, all with angular size larger than 3 arcmin, have been observed with the Fleurs Synthesis Telescope (FST) at 1415 MHz with a resolution of 22 arcsec. Spectral index differences within the sources were investigated by comparing 843 MHz images made with the Molonglo Observatory Synthesis Telescope (MOST) with FST images convolved to the same beam-size of 44 arcsec.

1. Introduction

The structure of selected radio sources in the southern sky has been explored with several radio telescopes, following the initial radio surveys that have been made for the Parkes Catalogue at 2·7 GHz (see Bolton *et al.* 1979) using the 64 m parabola, and the Molonglo Reference Catalogue (MRC) at 408 MHz using the Molonglo Cross Radio Telescope (Large *et al.* 1981, 1991). The largest sources discovered by these two general surveys have been imaged with the same telescopes using beamwidths of a few arcmin (Parkes: 4·1 arcmin at 5 GHz; e.g. Wall and Schilizzi 1979; and Molonglo: 2·9 arcmin at 408 MHz; e.g. Schilizzi and McAdam 1975). Images at a higher resolution of 1·9 arcmin have been published for many sources north of declination −45° using data from the Culgoora Radioheliograph at 160 MHz (Slee 1977) and, more recently, a complete sample of 91 southern radio galaxies has been investigated with the VLA at resolutions down to 0·7 arcsec (Ekers *et al.* 1989). The latter sample was selected from the Parkes 2·7 GHz survey and was restricted to declinations north of −40°. For sources in the far south, the Fleurs Synthesis Telescope (FST) provided high resolution images at 1415 MHz. In its early configuration, the FST had a beamwidth of ∼50 arcsec at 1415 MHz (Christiansen *et al.* 1977). The addition of six 13·7 m dishes to the array in 1985 improved the resolution to ∼20 arcsec (Bunton *et al.* 1985).

The present study using the upgraded FST complements a larger survey of southern radio galaxies (Jones and McAdam 1992). This survey used the Molonglo Observatory Synthesis Telescope (MOST, see Mills 1981; Robertson 1991) to observe extended sources south of declination −30° with a resolution of 44 arcsec at 843 MHz. This paper presents FST images at 1415 MHz for 23 particular interesting sources, for which higher resolution was required to explore compact hotspots, jets and cores.

0004-9506/92/060797$05.00

2. The Sources

The Molonglo Reference Catalogue (Large *et al.* 1981) noted extragalactic sources which were either extended (larger than ~1 arcmin) or multiple (within 8 arcmin of each other, and hence possibly two lobes of a single source). The positions, sizes and structures of 339 of these sources have been studied at 843 MHz with the Molonglo Observatory Synthesis Telescope (Jones 1989*a*; Jones and McAdam 1992). The MOST images defined a southern sample of 193 sources larger than 0·5 arcmin and stronger than 0·4 Jy (at 843 MHz). The sample includes almost all of the strong extended radio sources south of declination −30°. The discrepancy between the number of MRC sources observed and the final sample of 193 sources arises because many of the pairs of multiple sources were found to be lobes of the same source and pairs which were found to be unrelated random associations were excluded, as were the extended sources in the MRC found with the higher resolution to be groups of unrelated sources.

The FST targets were selected on the basis of the MOST observations, with an emphasis on sources newly recognised to have large angular size, and on the head–tail and twin-tail sources with very distorted structures.

3. Fleurs Observations

The Fleurs Observatory has been modified several times since it was established in the 1950s. In its final configuration, the array had 32 small (5·7 m) dishes in an east–west line and six large (13·7 m) dishes spread over 1585 m east–west and 587 m north–south (Jones *et al.* 1984; Bunton *et al.* 1985). The recorded data were, for convenience, divided into 15 correlations between all pairs of the six large dishes (called the Six-Dish Array) and 128 correlations between each of the 32 small dishes and the four large dishes on the same east–west line (East–West Array). The large dishes were under full computer control, and required much less effort to use than the small dishes which required manual setting up and checking throughout an observation.

Observations of 8 hours duration produced images by earth-rotation aperture synthesis, and were processed offline by the standard Fourier transform procedures (e.g. Perley *et al.* 1989).

The East–West Array had good uv coverage so that it produced a synthesised beam with low sidelobes, and had adequate short spacings to detect extended structure (Bunton *et al.* 1985). On the other hand the Six-Dish Array produced a beam with high sidelobes from sparse uv coverage omitting the short spacings (Batty *et al.* 1986). The combined data from both arrays gave the best results (provided the source of interest is near the field centre, as the arrays have different primary beams). In the present study, the full array was used for the observation of twelve sources, and the Six-Dish Array for the remaining eleven, as noted in Section 4.

The FST data were processed with the Fleurs Control Program (Sault 1984). The correlation data were edited, to remove interference and antenna tracking errors, and calibrated against observations of standard sources (usually 1934–638 which was taken to be 15·4 Jy at 1415 MHz). Images were produced by regridding, fast Fourier transforming the correlation data and cleaning. The restoring beam was a gaussian of half-power width $22\times22\,\mathrm{cosec}\delta$ arcsec^2, at declination δ. The cleaning used 250 components typically, which reached down to the noise level,

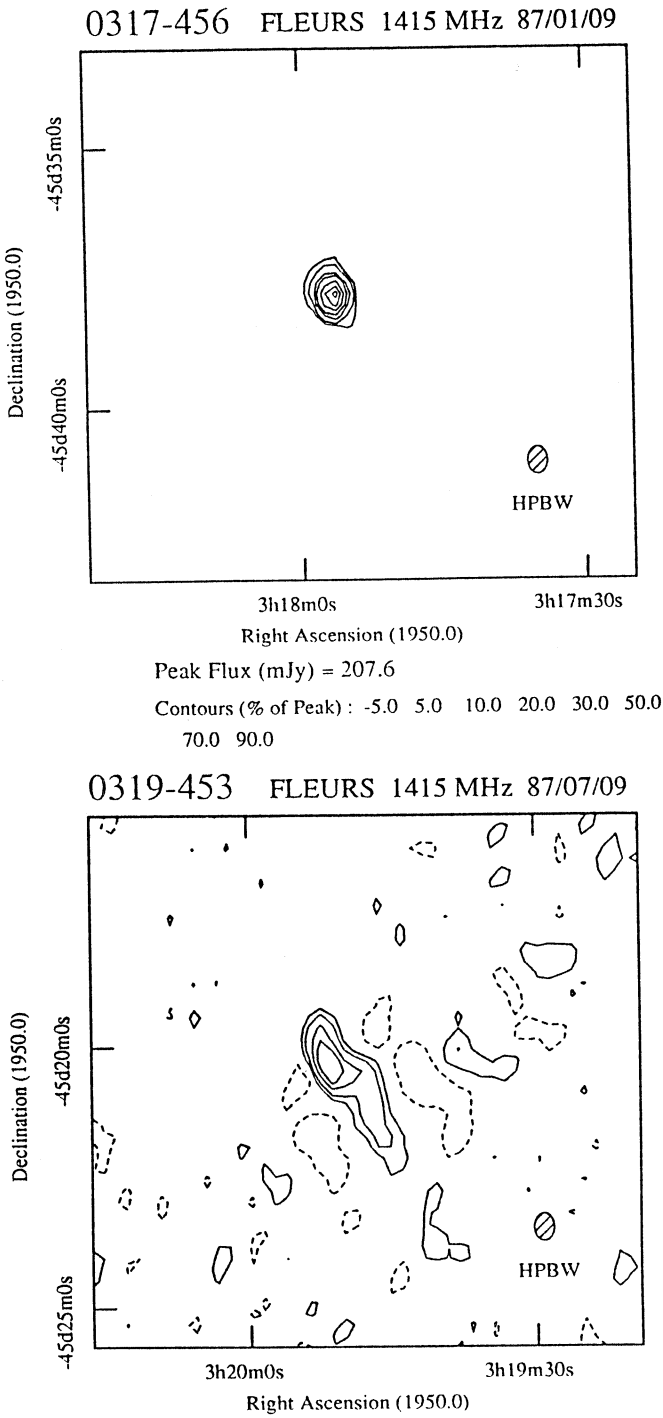

Fig. 1. The FST images at 1415 MHz with half-power beamwidth $22 \times 22 \operatorname{cosec}\delta$ arcsec^2.

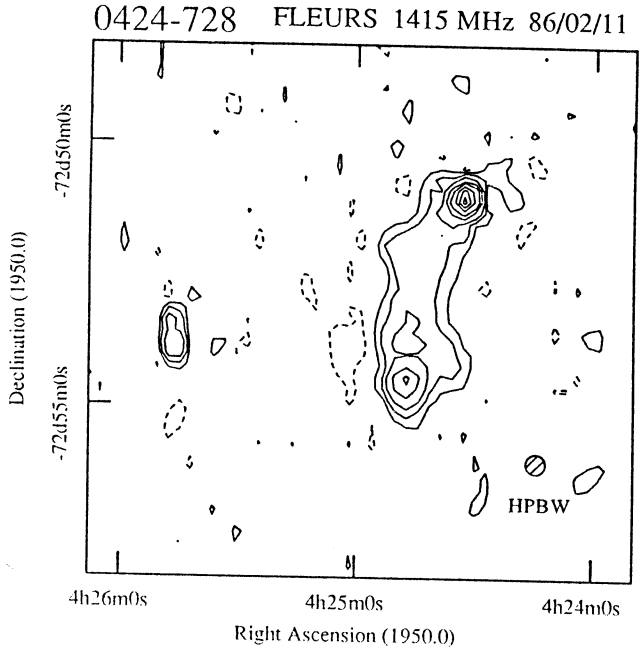

Peak Flux (mJy) = 316.3

Contours (% of Peak) : -2.0 2.0 5.0 10.0 20.0 30.0 50.0 70.0 90.0

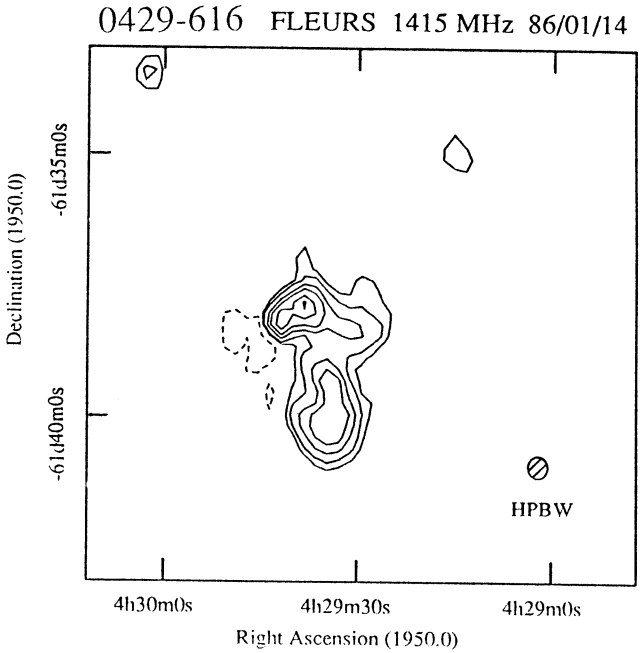

Peak Flux (mJy) = 208.8

Contours (% of Peak) : -5.0 5.0 10.0 20.0 30.0 50.0 70.0 90.0

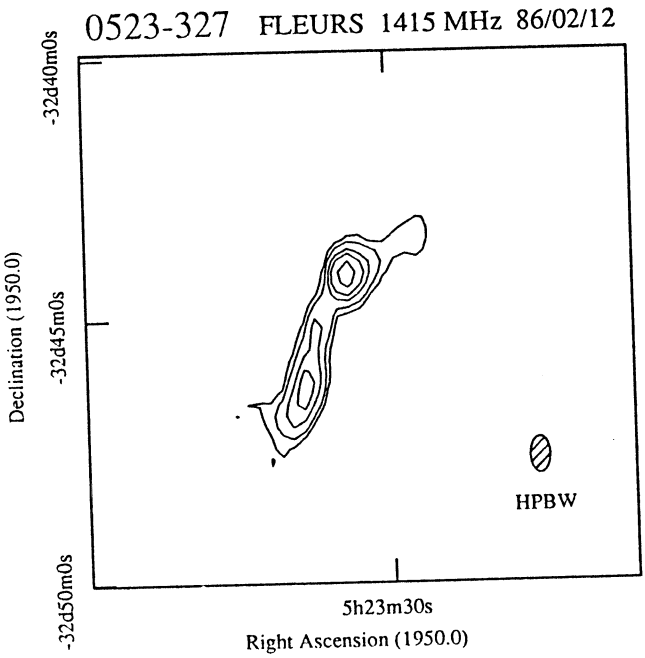

Peak Flux (mJy) = 303.6

Contours (% of Peak) : -5.0 5.0 10.0 20.0 30.0 50.0 70.0 90.0

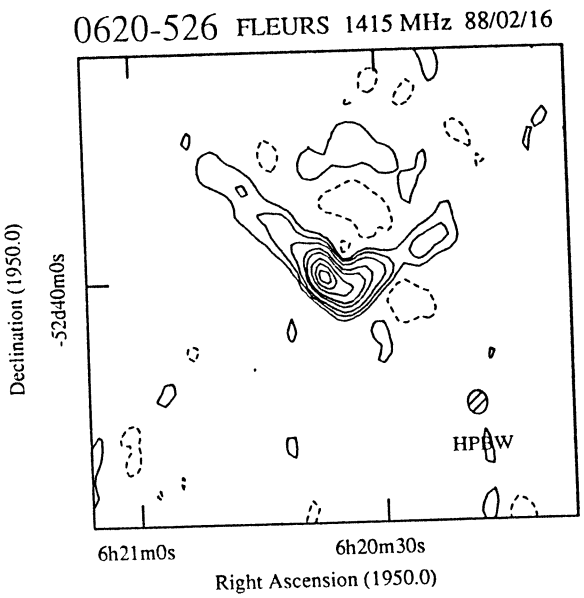

Peak Flux (mJy) = 761.2

Contours (% of Peak) : -2.0 2.0 5.0 10.0 20.0 30.0 50.0 70.0 90.0

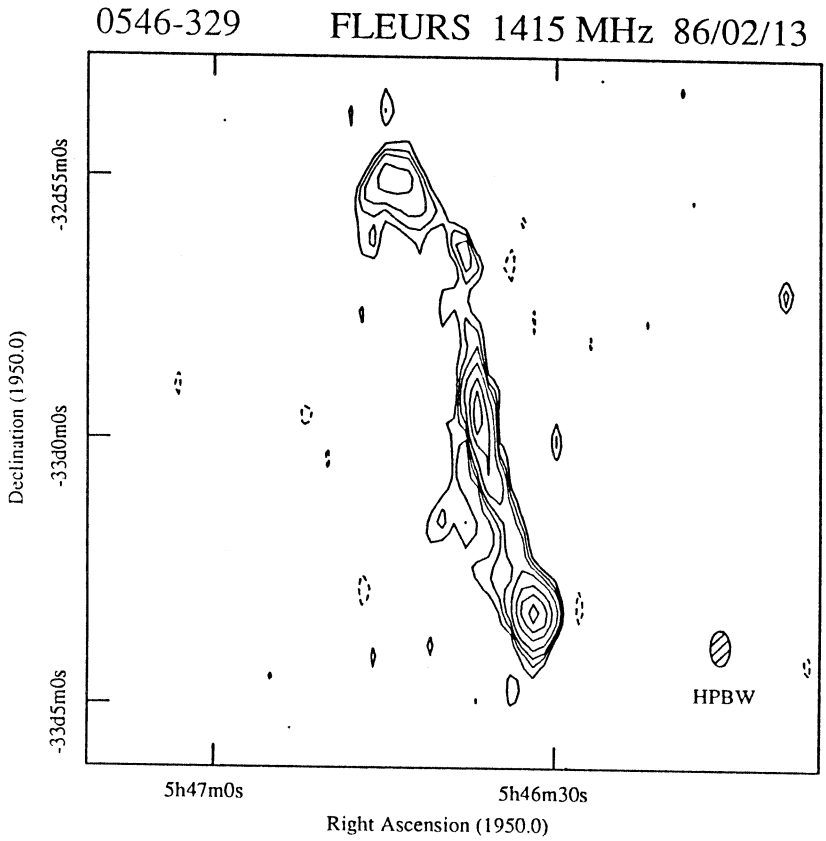

but some of the Six-Dish array observations of linear sources (e.g. 0319−453, 1137−463 and 1425−479) were difficult to clean, given the sparse uv coverage, and so still show residual sidelobes above the noise in the cleaned image. The cleaned images were plotted, with the lowest contour level (usually 5% of the peak) chosen to show the background noise.

The cleaned images are shown in Fig. 1. To appreciate the FST images in greater depth, the reader should compare them with the corresponding MOST images (Jones and McAdam 1992). The smaller beam area of the FST compared with the MOST shows finer structure in the the core, jet and hotspots. However, the broad lobe emission is seen less clearly than in the MOST images for three reasons: (a) typical extended structure has a steep spectrum ($\alpha \sim -0{\cdot}8$) so that the surface brightness falls by a factor of two between 843 and 1415 MHz; (b) the smaller beam area means that the flux per unit beam area is less by a factor of four; and (c) the FST has a smaller collecting area, and poorer noise figure, than the MOST. For the sources with full array observations (and hence good data at short uv spacings) an improved image of the broad-scale structure can be obtained by omitting the longer spacings and producing an image of reduced

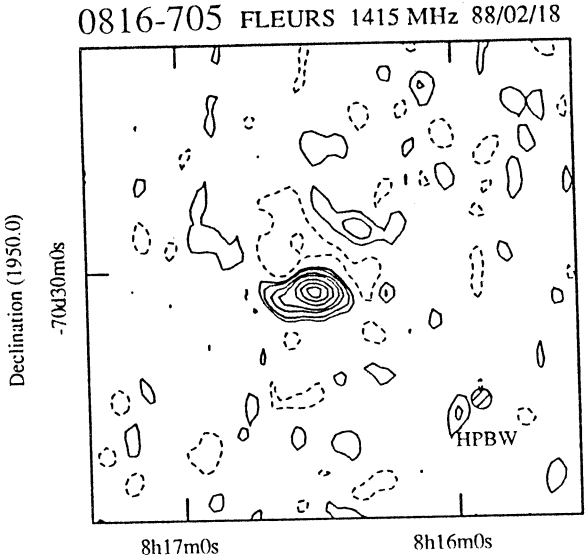

Peak Flux (mJy) = 185.6

Contours (% of Peak) : -5.0 5.0 10.0 20.0 30.0 50.0 70.0 90.0

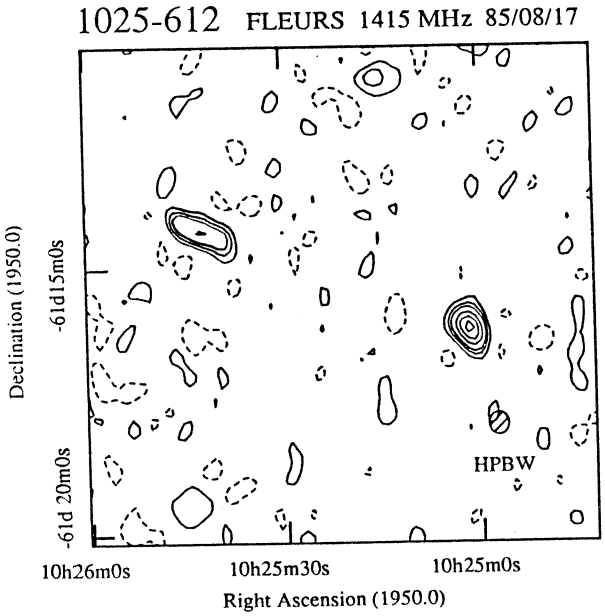

Peak Flux (mJy) = 66.49

Contours (% of Peak) : -10. 10.0 20.0 30.0 50.0 70.0 90.0

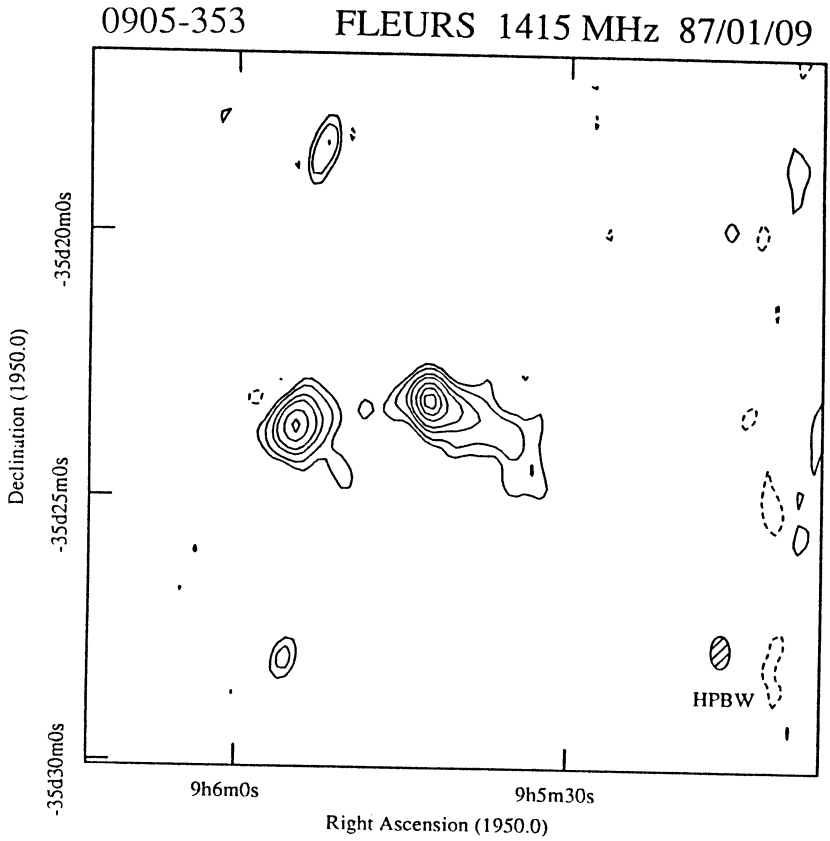

resolution with a cleaned beam of $44\times44\,\mathrm{cosec}\delta$ arcsec^2 to match the MOST resolution and counteract the factor (b) above. These images (Jones 1989*a*) are not given here, since they are very similar in appearance to the MOST images (Jones and McAdam 1992), as expected from the matched resolution, but with lower dynamic range. Detailed comparison with the MOST images does show differences due to spectral index differences within the sources.

The integrated flux densities and peak positions obtained from the FST images are given in Table 1. For sources with full array data, the integrated flux densities were obtained (by pixel summation) from the lower 44 arcsec resolution images since these show low surface brightness emission better. The integrated flux densities from Six-Dish Array data (shown within parentheses in Table 1) are known to be too low because of missing short uv spacings.

Even for the sources with full array data the integrated flux densities from the FST images are lower by ~15% than either the flux densities from the Parkes 64 m telescope at 1410 MHz or the interpolation of data from other frequencies. This is partly due to the difficulty of integrating the low brightness emission, and partly due to uncertainties in the flux calibration of the observations. It was

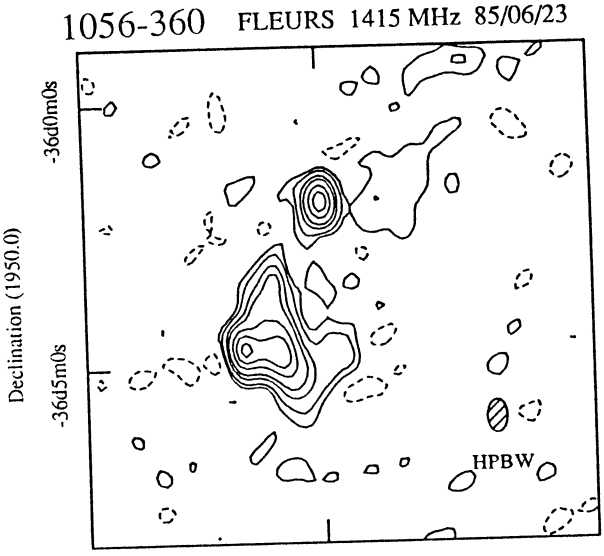

Peak Flux (mJy) = 114.7

Contours (% of Peak) : -5.0 5.0 10.0 20.0 30.0 50.0 70.0 90.0

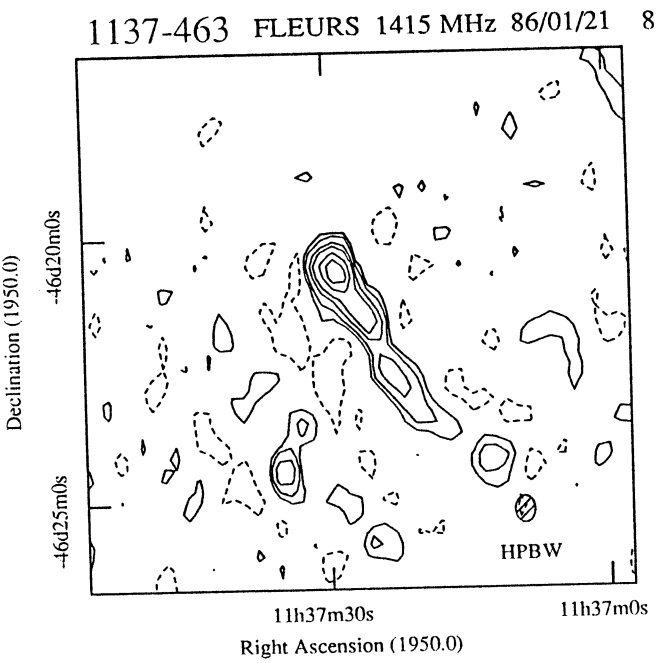

Peak Flux (mJy) = 144.5

Contours (% of Peak) : -5.0 5.0 10.0 20.0 30.0 50.0 70.0 90.0

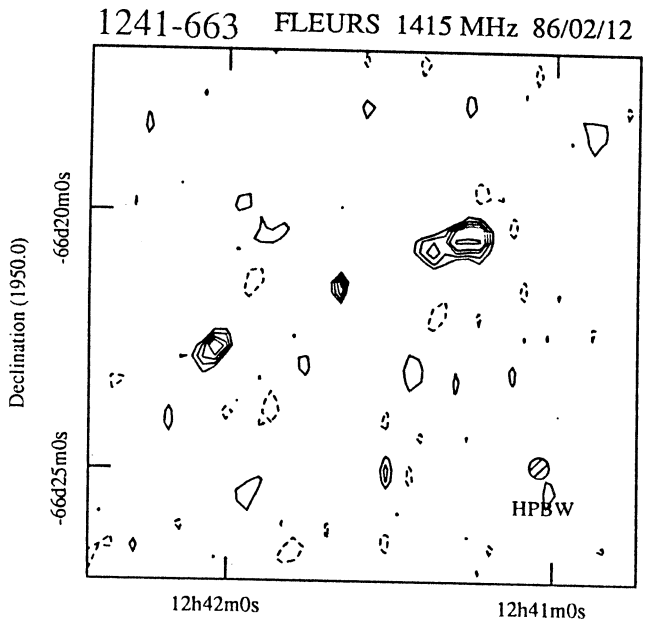

Peak Flux (mJy) = 33.67

Contours (% of Peak) : -20. 20.0 30.0 40.0 50.0 70.0 90.0

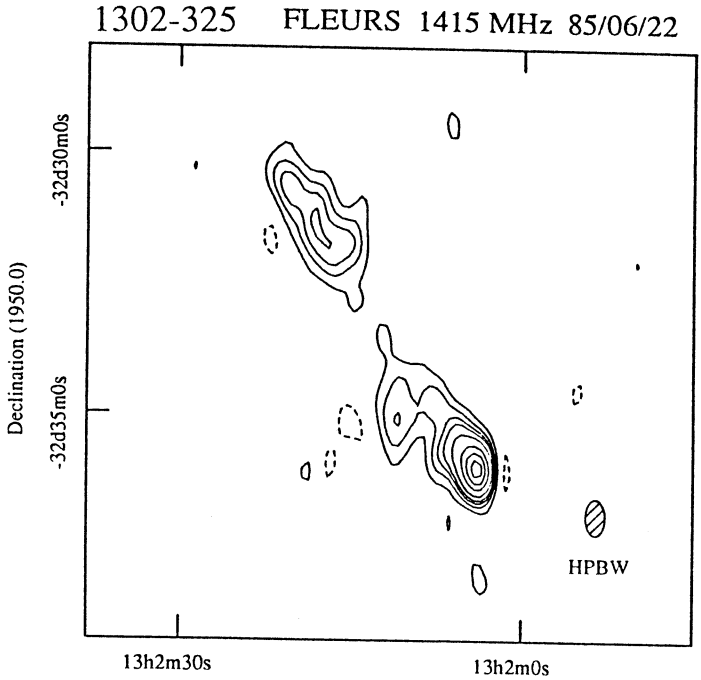

Peak Flux (mJy) = 184.3

Contours (% of Peak) : -5.0 5.0 10.0 15.0 20.0 30.0 50.0 70.0 90.0

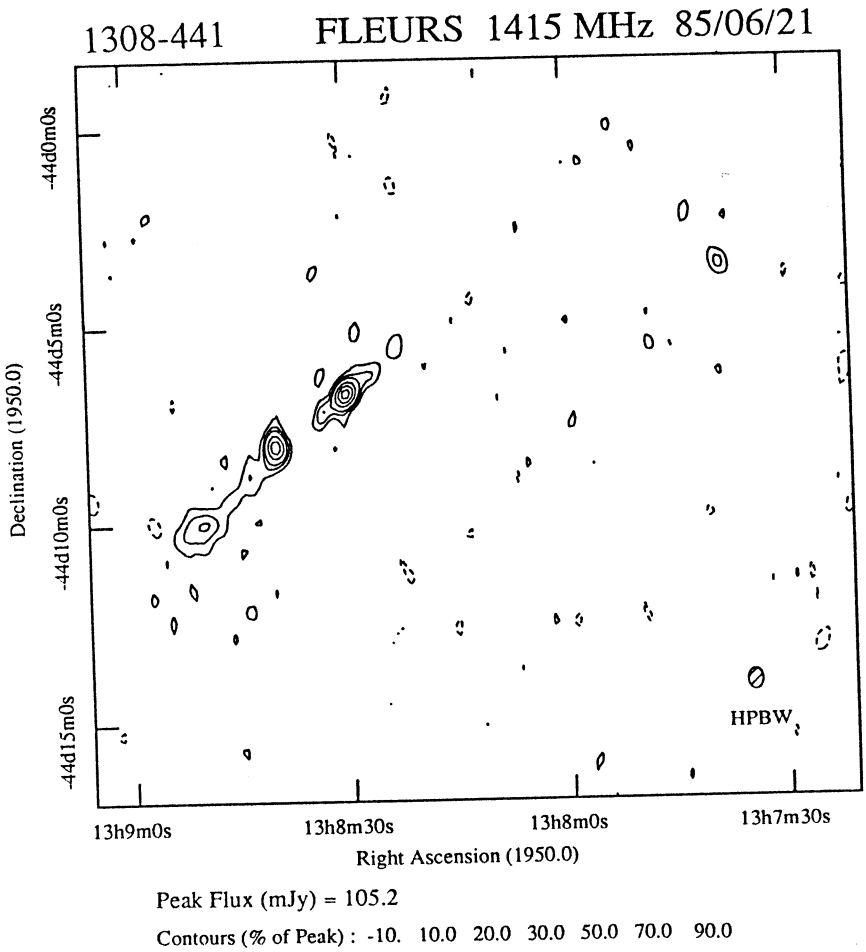

found that the pixel summation to obtain integrated fluxes was very sensitive to the assumed baselevel, since large areas of low surface brightness emission were being integrated. This is why low resolution images were used to obtain integrated fluxes—the high resolution images gave lower, and more uncertain, fluxes even though they used the same raw data.

The spectral indices between 843 and 1415 MHz obtained from the comparison of MOST and FST integrated fluxes are unreliable, due to these problems with the FST integrated fluxes, and hence are not quoted here. However, the *relative* spectral index differences across the sources ($\Delta\alpha$) are more reliable and are given in Section 4. The spectral index differences were obtained by comparing the peak brightnesses of different components of the same source in the MOST and FST (44 arcsec) images. This bypasses most of the problems with pixel summation and absolute calibration of the FST images. The major source of uncertainty in the spectral index differences is noise in the FST images (estimated at 3 mJy/beam for the 22 arcsec and 5 mJy/beam for the 44 arcsec images). The noise in the MOST images is less than 1 mJy/beam, and the absolute calibration errors cancel out since only relative fluxes are used.

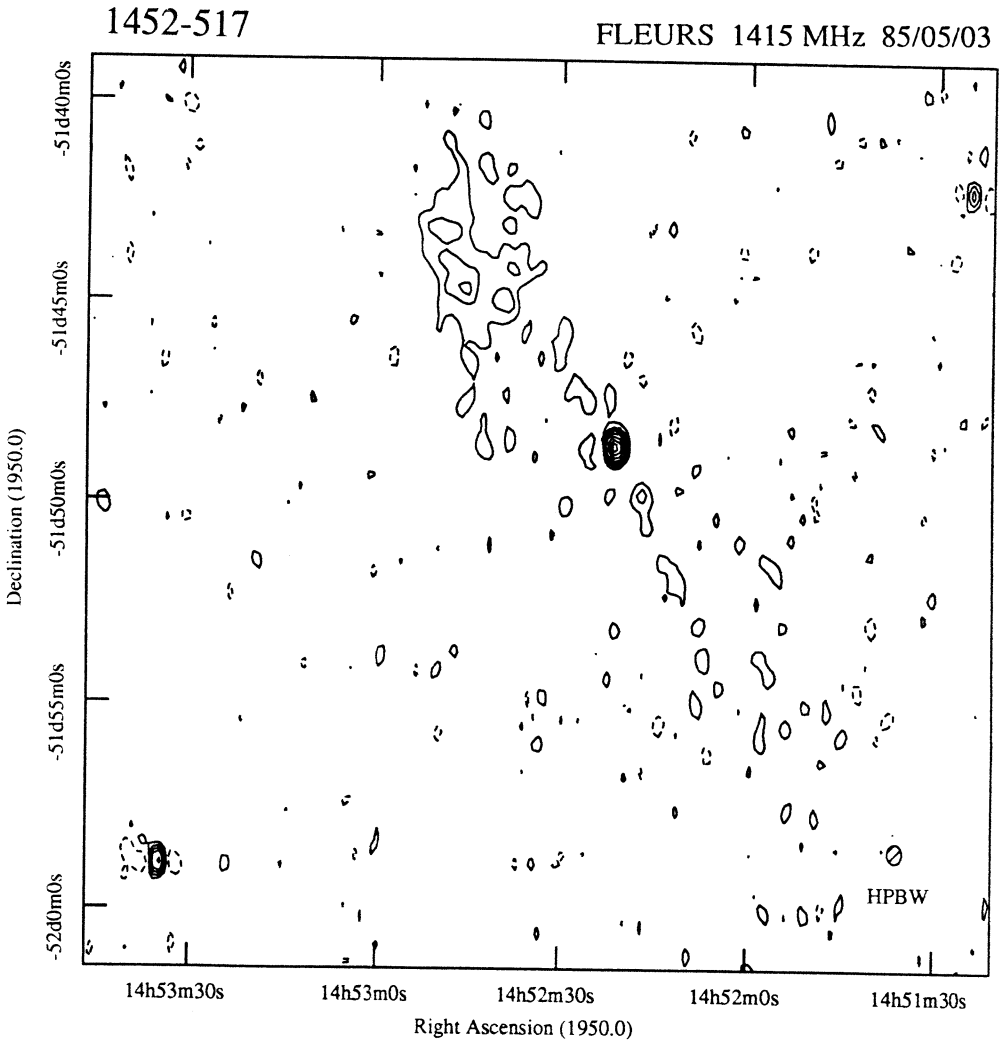

The positions in Table 1 are the peaks of brightness in the 22 arcsec images, showing the cores and the hotspots in the lobes. The uncertainty in FST positions is around 2 arcsec (Bunton *et al.* 1985). Centroid positions were not used, due to the missing short spacings and the difficulty of integrating low brightness emission.

4. Discussion

The following notes on individual sources concentrate on (1) the comparison of the FST and MOST images, (2) details of the structure revealed with the higher resolution of the FST (22 arcsec beamwidth), and (3) the spectral index differences revealed by using the synthesised beams of 44 arcsec at two different

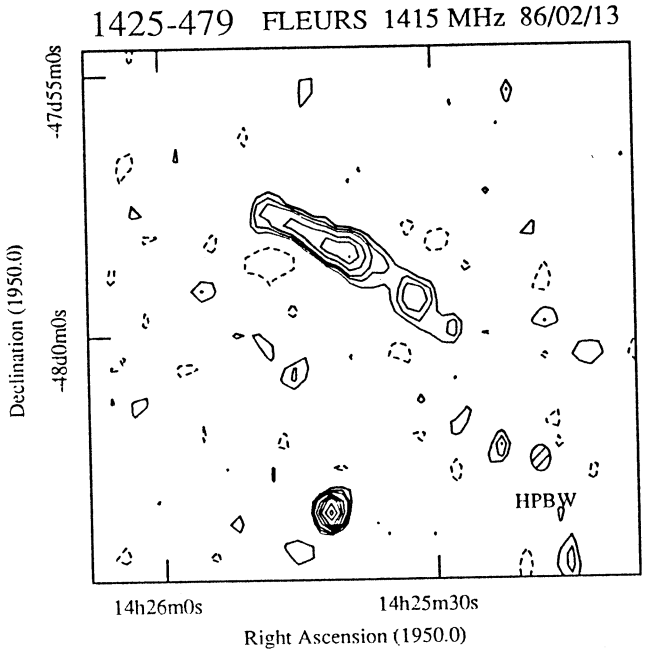

Peak Flux (mJy) = 76.40

Contours (% of Peak) : -10. 10.0 15.0 20.0 30.0 40.0 50.0 70.0 90.0

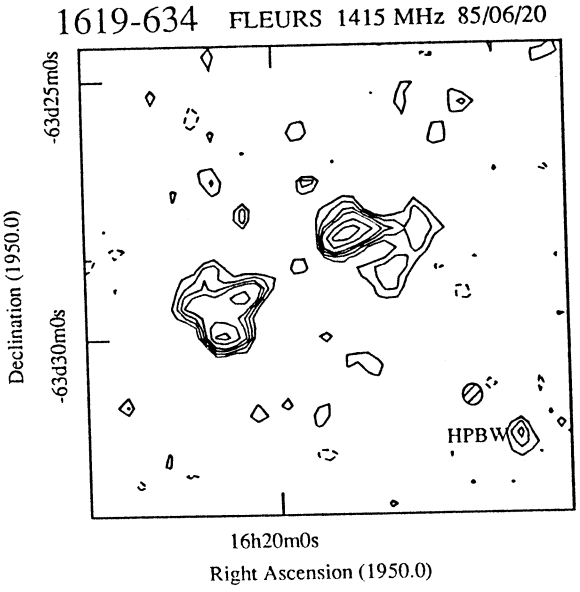

Peak Flux (mJy) = 34.29

Contours (% of Peak) : -20. 20.0 30.0 40.0 50.0 70.0 90.0

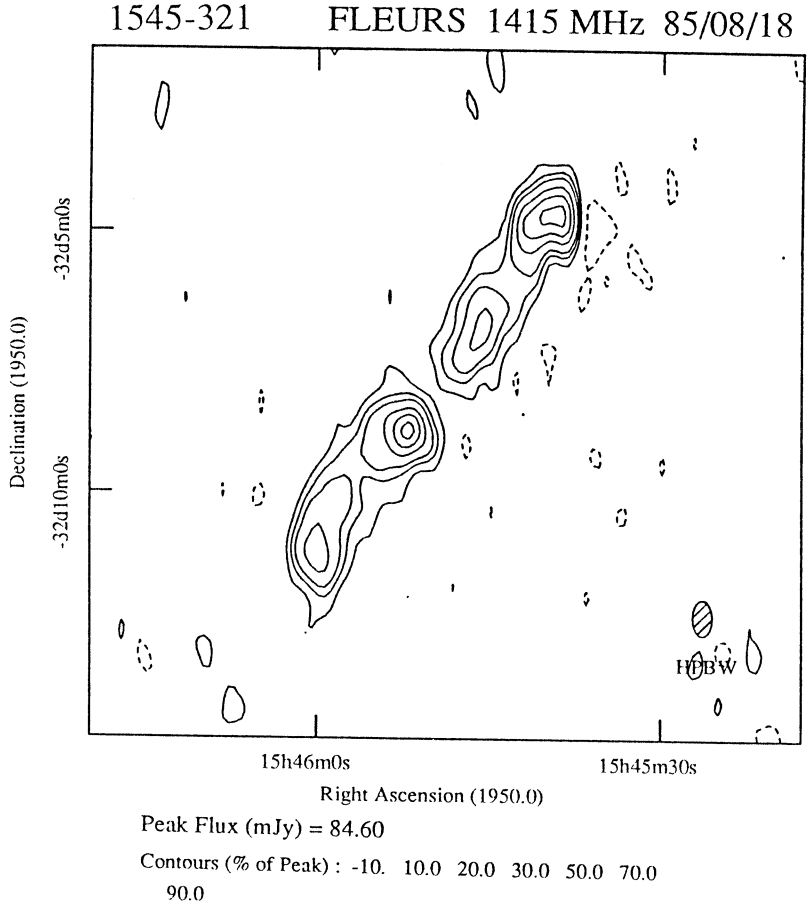

frequencies. Further details on the sources, such as the optical identifications and references to other observations, are given with the MOST images by Jones and McAdam (1992).

0317–456, 0319–453. The two lobes of this giant radio galaxy were observed separately since the source size is nearly half the primary beamwidth. The observations were made with the Six-Dish Array and omit much of the extended structure. The south–west lobe (0317–456) shows only the compact hotspot, which is smaller than the 22 arcsec beam, and none of the low-level extended structure seen on the MOST image. The north–east lobe (0319–453) shows only a weak bent structure near the sharp east edge of the strong extended emission in the MOST image (the more easterly of the two peaks). This is, perhaps, a hotspot where the jet is stopped in the intergalactic medium and powers the lobes. The offset position and kink suggest a deflection of the jet as it is being decelerated. This source is discussed in more detail in Jones (1989*b*).

0424–728 (full array). The double is edge-brightened, with prominent, compact hotspots, particularly in the north lobe. The extended structure shows some rotational symmetry with projections on the north–east and south–west. The

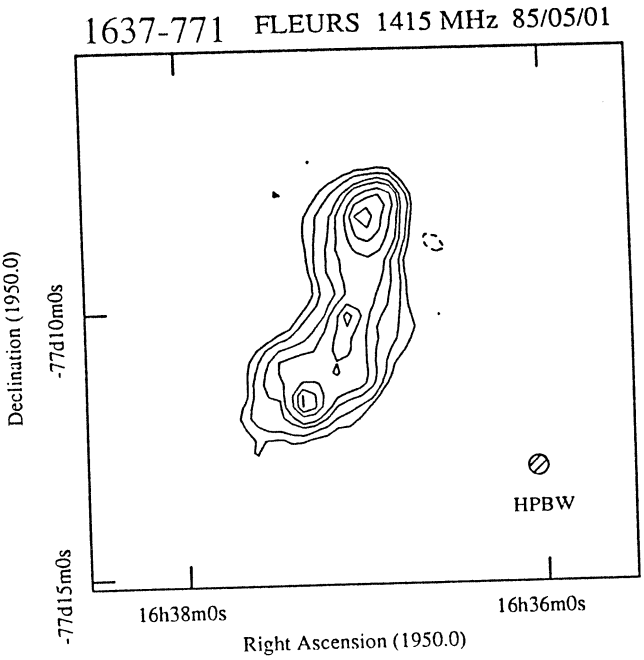

Peak Flux (mJy) = 348.7

Contours (% of Peak) : -5.0 5.0 10.0 20.0 30.0 50.0 70.0 90.0

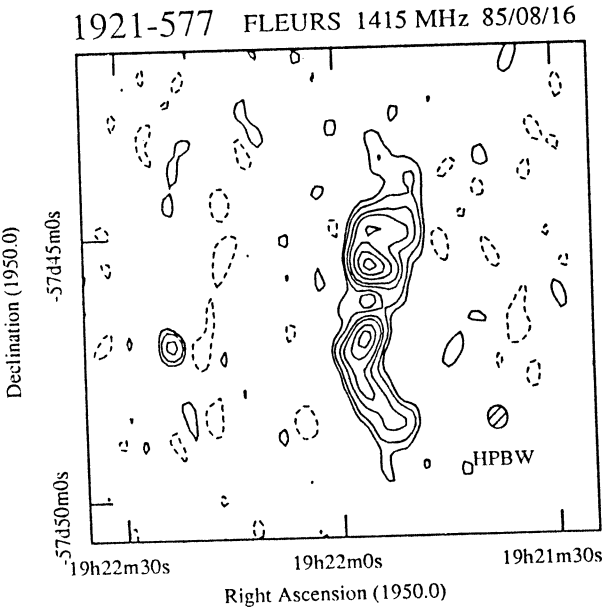

Peak Flux (mJy) = 129.8

Contours (% of Peak) : -5.0 5.0 10.0 20.0 30.0 50.0 70.0 90.0

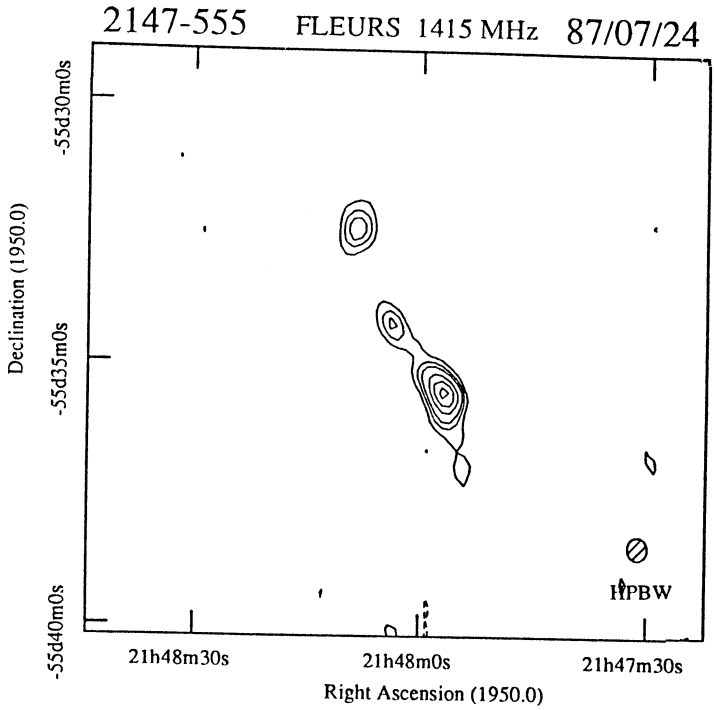

Peak Flux (mJy) = 211.3

Contours (% of Peak) : -10. 10.0 20.0 30.0 50.0 70.0 90.0

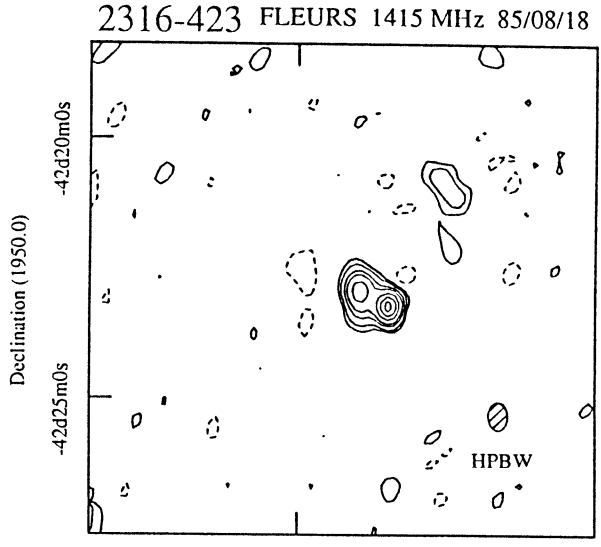

Peak Flux (mJy) = 229.3

Contours (% of Peak) : -5.0 5.0 10.0 20.0 30.0 50.0 70.0 90.0

Table 1. Summary of integrated flux densities, peak positions and peak brightnesses from the FST images

The integrated flux densities are low due to missing short spacings for the Six-Dish Array observations in parentheses

Source	Integrated flux density S_{1415}/Jy	Peak position right asc. h m s	declin. ° ′ ″	Peak brightness Jy/beam
0317–456	(0·26)	03 17 56·3	−45 37 48	0·21
0319–453	(0·155)	03 19 51·1	−45 20 26	0·070
0424–728	1·33	04 24 32·6	−72 51 05	0·32
		04 24 47·1	−72 54 30	0·104
0429–616	1·47	04 29 34·4	−61 40 04	0·096
		04 29 38·4	−61 37 58	0·157
0523–327	0·94	05 23 33·6	−32 44 08	0·21
		05 23 37·6	−32 46 25	0·123
0546–329	1·00	05 46 31·8	−33 03 16	0·078
		05 46 36·9	−32 59 29	0·069
		05 46 44·7	−32 55 02	0·030
0620–526	(2·38)	06 20 36·9	−52 39 53	0·77
0816–705	(0·44)	08 16 30·5	−70 30 24	0·189
0905–353	(0·94)	09 05 42·3	−35 23 12	0·22
		09 05 54·7	−35 23 40	0·163
1025–612	(0·24)	10 25 01·6	−61 16 11	0·068
		10 25 42·4	−61 14 18	0·036
1056–360	1·10	10 56 29·9	−36 01 53	0·101
		10 56 36·9	−36 04 40	0·116
1137–463	(0·47)	11 37 29·2	−46 20 35	0·132
1241–663	(0·166)	12 41 17·1	−66 20 33	0·027
		12 41 39·3	−66 21 26	0·019
		12 42 02·2	−66 22 41	0·024
1302–325	0·90	13 02 04·1	−32 35 59	0·188
		13 02 10·9	−32 35 07	0·029
		13 02 18·1	−32 31 22	0·039
1308–441	0·68	13 07 38·5	−44 03 30	0·026
		13 08 30·0	−44 06 41	0·107
		13 08 39·6	−44 08 04	0·088
		13 08 49·7	−44 09 59	0·034
1425–479	(0·22)	14 25 31·7	−47 59 21	0·021
		14 25 41·1	−47 58 17	0·041
1452–517	3·56	14 52 21·3	−51 48 39	0·142
1545–321	1·41	15 45 38·9	−32 04 42	0·084
		15 45 45·6	−32 06 48	0·052
		15 45 52·1	−32 08 48	0·085
		15 45 59·7	−32 11 15	0·051
1619–634	0·65	16 19 47·4	−63 27 56	0·035
		16 20 08·2	−63 29 57	0·034
1637–771	6·8	16 36 57·9	−77 08 14	0·35
		16 37 05·1	−77 10 09	0·28
		16 37 19·5	−77 11 46	0·34
1921–577	1·05	19 21 55·4	−57 45 35	0·132
		19 21 56·5	−57 47 00	0·109
2147–555	(0·89)	21 47 56·9	−55 35 35	0·22
		21 48 03·6	−55 34 17	0·073
		21 48 08·5	−55 32 28	0·086
2316–423	(0·42)	23 16 20·9	−42 23 15	0·23
		21 16 23·6	−42 22 55	0·154

nearby source to the east is extended with a similar position angle. The northern lobe has a flatter spectrum than the southern ($\Delta\alpha = 0{\cdot}22 \pm 0{\cdot}06$), probably due to the more prominent (flat spectrum) hotspot.

0429–616 (full array). The double is edge-brightened with a large amount of distortion in the north lobe. The optical identification (Jones and McAdam 1992), in Abell cluster 3266 (Abell *et al.* 1989), is near the distorted ridge-line, although far from the centroid. The 44 arcsec FST image, like the MOST image, shows the east side of the extended emission has a sharper edge than the north–west. The north lobe has a flatter spectrum than the south ($\Delta\alpha = 0{\cdot}12 \pm 0{\cdot}05$).

0523–327 (full array). The south lobe is long and narrow, while the north lobe is more compact, with an extension to the west (see also the VLA image by Ekers *et al.* 1989). The 44 arcsec FST image shows an S-shape with low brightness projections to the south–east as well as the north–west, as in the MOST image. These projections have a steeper spectrum than the rest of the source. The south lobe has a flatter spectrum than the north ($\Delta\alpha = 0{\cdot}18 \pm 0{\cdot}05$).

0546–329 (full array). Edge-brightened source with narrow jets connecting the core to hotspots in the lobes, the north jet bent to the east. The lobes have steeper spectra than the core, and the north lobe is steeper than the south ($\Delta\alpha = -0{\cdot}99 \pm 0{\cdot}14$ and $\Delta\alpha = -0{\cdot}38 \pm 0{\cdot}10$ respectively from the core). The diffuse emission to the east of the lobes in the MOST image has an even steeper spectrum. Higher resolution VLA images of the core and jet were given in Ekers *et al.* (1989).

0620–526 (Six-Dish Array). This wide-angle-tail source is bent nearly at a right angle near the peak, with narrow and straight lobes. The optical galaxy is close to the peak of the radio source.

0816–705 (Six-Dish Array). The peak of this twin-tail source is extended east–west, but the tails trailing off to the north and west, seen well on the MOST image, only just appear above the noise level. The lack of short spacings means extended structure is missing.

0905–353 (Six-Dish Array). The hotspots of the two lobes are detected, the east is extended, and the west lobe trails off to the west and then to the south. There are two small, weak sources nearby nearly in a line with the east hotspot, but the alignment is probably coincidental.

1025–612 (Six-Dish Array, only five dishes used). The west lobe has a bright hotspot (position angle 30°) and the east lobe is narrow and elongated. The core seen on the MOST image is not detected (< 7 mJy at 1415 MHz) and so has a steep spectrum.

1056–360 (full array). The south lobe shows double structure at the peak, plus distorted low-level structure to the south and west. The north lobe shows a compact hotspot, with low-level diffuse structure (nearly lost in the noise) to the west. The projection on the north side of the south lobe is consistent with the optical identification midway between the hotspots. The source does not fit neatly into the Fanaroff and Riley (FR; 1974) classification scheme, having prominent hotspots but diffuse emission further out. It may be a transition source as its power is close to the FR break. The peaks of the two lobes have the same spectral indices (within 0·1), but the diffuse structure to the north–west has a substantially steeper spectrum ($\Delta\alpha = -0{\cdot}4 \pm 0{\cdot}2$). The VLA image of Ekers *et al.* (1989) shows the compact hotspots, a weak core component and some of the diffuse emission.

1137–463 (Six-Dish Array, average of two observations). This head–tail source shows a narrow tail, but the weak extension seen to the east in the MOST image is not detected in the FST image. The tail in the FST image has several peaks, showing a more knotty structure than the smooth variation in the MOST image (even when the difference in resolution is taken into account), suggesting spectral index differences. For example, the point where the tail bends on the MOST image is a peak in the FST image, so it has a flatter spectrum. The peak to the south–east is considered an unrelated source.

1241–663 (Six-Dish Array). Only the hotspots in each lobe and core are seen in the FST image: the extended structure seen in the MOST image is not detected due to the missing short spacings and the lower sensitivity. The west hotspot is extended along the source major axis or is double.

1302–325 (full array). The south lobe has a prominent hotspot near the end but the north lobe has no obvious hotspot. The structure is linear except for the weak extended component on the north–east of the south lobe. The lobes have the same spectral indices (within 0·1), while the bridge emission has a flatter spectrum and the north–east peak on the south lobe a steeper spectrum.

1308–441 (full array). The four strongest peaks of this complex source are detected: the core, the bright spot on the south–east jet, the south–east lobe and the hotspot at the end of the north–west lobe (only just above the noise level). The core is extended in the direction of the source major axis with the inner parts of the two jets. The low brightness structure, seen in the MOST image to link these components, is not detected. The core, the south–east lobe and south–east bright spot have the same (steep) spectra (within 0·15) and the hotspot on the north–west lobe a much flatter spectrum ($\Delta\alpha = 0{\cdot}7 \pm 0{\cdot}3$). This source is discussed in more detail in Jones (1987) where the low resolution FST image is shown. This indicates that the north–west ridge line seen in the MOST image has a steep spectrum, as it is not seen in the FST image.

1425–479 (Six-Dish Array). The two lobes are narrow and edge-darkened, with a slight bend. The source to the south is unresolved, and assumed to be unrelated.

1452–517 (full array). The core is slightly extended north–south. The extended lobes seen on the MOST image are detected on the FST image, but the south lobe is only just above the noise level. The core has a flat spectrum with the peak of the north lobe having a steeper spectrum ($\Delta\alpha = -0{\cdot}57 \pm 0{\cdot}12$ compared to the core). The south lobe also appears to have a steeper spectrum than the core ($\Delta\alpha = -0{\cdot}4 \pm 0{\cdot}3$), but this is less clear due to the low surface brightness. This source is discussed in Jones (1986), where the low resolution FST image is shown, and in Jones (1989*b*).

1545–321 (full array). Both lobes have compact structure on the north–west side with the south–east side more elongated. This is an unusual symmetry for a radio galaxy—the compact hotspots are usually at the ends of the lobes (for an FR II source). The ridge-line has a slight bend. Three of the four components have similar spectral indices, with the north–west peak slightly flatter ($\Delta\alpha = 0{\cdot}16 \pm 0{\cdot}07$).

1619–634 (full array). The source shows distorted structure in both lobes. The east lobe has the hotspot to the south of the axis with low brightness structure to the north. The west lobe has structure to the west which then bends to the

south–east. The peak of the west lobe has a flatter spectrum ($\Delta\alpha = 0{\cdot}3 \pm 0{\cdot}2$) than the east.

1637–771 (full array). The lobes have compact hotspots near (but not at) their ends. The core is detected as a slight peak on the bent bridge emission. The north lobe has a flatter spectrum than the south ($\Delta\alpha = 0{\cdot}19 \pm 0{\cdot}02$).

1921–577 (full array). The two lobes are edge-darkened and bent towards the west. The south lobe is narrow. The bending of the inner lobes is consistent with the optical identification to the west of these two peaks, implying the lobes first bend towards the east as they come from the galaxy. The north lobe has a flatter spectrum than the south ($\Delta\alpha = 0{\cdot}13 \pm 0{\cdot}06$).

2147–555 (Six-Dish Array). Only the core and inner lobes of this edge-darkened source are seen on the FST image. The outer lobes seen on the MOST image are not detected due to the missing short spacings and lower sensitivity. The core and inner lobes are elongated in the direction of the (bent) ridge-line of the source.

2316–423 (Six-Dish Array, only five dishes used). The head of this twin-tail source is resolved into a double, with the brighter component coinciding with the optical galaxy. (The feature to the north–west is probably a residual of the dirty-beam sidelobe as it does not correspond to the diffuse emission in the MOST image.) See also the VLA image of Hjellming and Bignell (1982).

The FST images at a resolution of 22 arcsec show more compact structure in the core, jets and lobe hotspots than can be seen in the MOST 44 arcsec resolution images. Even in sources where the lobes are diffuse, compact structure is revealed. However, the higher resolution observations miss out some of the diffuse emission since as the beam area is reduced, the flux per beam falls and the low surface brightness structure is lost in the noise. In order to interpret the structure within a source it is necessary to use observations of several different resolutions to match the scales of the structures of interest.

Comparison of the images at the same resolution (44 arcsec) at the two different frequencies of the FST and MOST shows spectral index differences between the two lobes and the core. The data presented here did not allow the spectral index to be mapped accurately over the sources, but spectral index mapping is an important tool in determining how the synchrotron emission over the source is powered. There is evidence of asymmetry in the spectral index as well as in the structure of the two lobes.

5. Epilogue

The Fleurs Synthesis Telescope was developed by the School of Electrical Engineering, University of Sydney from the original array of the CSIRO Division of Radiophysics. For many years, it was the highest resolution telescope available for the far southern sky (50 arcsec in the late 1970s and 20 arcsec in the mid 1980s), although the Very Large Array (VLA) can reach declination $-45°$ (Hjellming and Bignell 1982) and has observed sources over much of the southern sky (Ekers *et al.* 1989). The need for a versatile radio telescope with arcsecond resolution to observe the far south (e.g. the Magellanic Clouds) is now satisfied by the Australia Telescope (AT, Norris 1988). The FST was shut down in 1988, around the time the AT was opened. The Fleurs Observatory was transferred

to the University of Western Sydney in 1991, and the six dishes are returning to operation as the Fleurs Student Radio Telescope.

Acknowledgments

I would like to thank the staff of the School of Electrical Engineering, University of Sydney, particularly David Brown, John Bunton and Julian Corben, for help with the FST observations and data reduction. I also thank Bruce McAdam and Lawrence Cram for their helpful comments.

References

Abell, G. O., Corwin, H. G., and Olowin, R. (1989). *Astrophys. J. Suppl.* **70**, 1.
Batty, M. J., Bunton, J. D., Brown, D. R., Corben, J. B., and White, G. L. (1986). *Proc. Astron. Soc. Aust.* **6**, 346.
Bolton, J. G., Savage, A., and Wright, A. E. (1979). *Aust. J. Phys. Astrophys. Suppl.* No. 46.
Bunton, J. D., Jones, I. G., and Brown, D. R. (1985). *Proc. Astron. Soc. Aust.* **6**, 93.
Christiansen, W. N., Frater, R. H., Watkinson, A., O'Sullivan, J. D., Lockhart, I. A., and Goss, W. M. (1977). *Mon. Not. R. Astron. Soc.* **181**, 183.
Ekers, R. D., *et al.* (1989). *Mon. Not. R. Astron. Soc.* **236**, 737.
Fanaroff, B. L., and Riley, J. M. (1974). *Mon. Not. R. Astron. Soc.* **167**, 31p.
Hjellming, R. M., and Bignell, R. C. (1982). *Science* **216**, 1279.
Jones, I. G., Watkinson, A., Egau, P. C., Percival, T. M., Skellern, D. J., and Graves, G. R. (1984). *Proc. Astron. Soc. Aust.* **5**, 574.
Jones, P. A. (1986). *Proc. Astron. Soc. Aust.* **6**, 329.
Jones, P. A. (1987). *Proc. Astron. Soc. Aust.* **7**, 208.
Jones, P. A. (1989*a*). Ph.D. Thesis, University of Sydney.
Jones, P. A. (1989*b*). *Proc. Astron. Soc. Aust.* **8**, 81.
Jones, P. A., and McAdam, W. B. (1992). *Astrophys. J. Suppl.* **80**, 137.
Large, M. I., Cram, L. E., and Burgess, A. M. (1991). *Observatory* **111**, 72.
Large, M. I., Mills, B. Y., Little, A. G., Crawford, D. F., and Sutton, J. M. (1981). *Mon. Not. R. Astron. Soc.* **194**, 693.
Mills, B. Y. (1981). *Proc. Astron. Soc. Aust.* **4**, 156.
Norris, R. P. (1988). *Sky & Telescope* **76**, 615.
Perley, R. A., Schwab, F. R., and Bridle, A. H. (Eds) (1989). 'Synthesis Imaging in Radio Astronomy', ASP Conf. Ser. 6.
Robertson, J. G. (1991). *Aust. J. Phys.* **44**, 729.
Sault, R. J. (1984). *In* 'Indirect Imaging' (Ed. J. A. Roberts), p. 367 (Cambridge Univ. Press).
Schilizzi, R. T., and McAdam, W. B. (1975). *Mem. R. Astron. Soc.* **79**, 1.
Slee, O. B. (1977). *Aust. J. Phys. Astrophys. Suppl.* No. 43.
Wall, J. V., and Schilizzi, R. T. (1979). *Mon. Not. R. Astron. Soc.* **189**, 593.

Manuscript received 21 July, accepted 15 October 1992